

6th CIRP Conference on Surface Integrity

Tool development for hybrid finishing milling of iron aluminides

Julien Witte^{a, *}, Dirk Schroepfer^a, Martin Hamacher^b, Heiner Michels^b, Christoph Hamm^c, Michael Appelt^d, Andreas Boerner^a, Thomas Kannengiesser^a

^aDepartment 9 – Component Safety, Bundesanstalt für Materialforschung und -prüfung (BAM), Unter den Eichen 87, 12205 Berlin, Germany

^bAccess e.V., Intzestr. 5, 52072 Aachen, Germany

^cWOLF Werkzeugtechnologie GmbH, 66892 Bruchmühlbach-Miesau, Germany

^dAWB GmbH, 68623 Lampertheim, Germany

* Julien Witte. Tel.: 0049 30 8104-3954; E-mail address: julien.witte@bam.de

Abstract

The importance of high-temperature materials made of iron aluminides (FeAl) has been increasing in light weight applications, e.g., airplane turbines, due to the high material's specific strength. However, the highly economic production by means of permanent mold casting involves special microstructures for Fe26Al4Mo0.5Ti1B alloy components leading to difficult machinability for subsequent finishing milling and low surface qualities. Major effects of tool and machining parameter variation incorporating ultrasonic assistance on the milling process and surface integrity are shown. Loads for tool and component surface are significantly adjustable to enable an economic process chain regarding the surface integrity of safety-relevant components.

© 2022 The Authors. Published by ELSEVIER B.V.

This is an open access article under the CC BY-NC-ND license (<https://creativecommons.org/licenses/by-nc-nd/4.0>)

Peer review under the responsibility of the scientific committee of the 6th CIRP CSI 2022

Keywords: Ultrasonic-assisted milling; Iron aluminide; Surface integrity; Tool wear

Nomenclature

a_e	width of cut (step over)
a_p	depth of cut
CM	conventional milling
D_t	milling tool diameter
F_r	resulting force
F_f	feed force in x-direction
F_{fN}	feed normal force in y-direction
F_p	passive force in z-direction
f_z	feed per cutting edge
K_{IC}	fracture toughness according to Shetty
n	rotational speed
R_a	average surface roughness
r_β	cutting edge rounding
S_a	arithmetical mean height of the surface (area)
S_{pk}	reduced peak height

USAM	ultrasonic-assisted milling
VB_{max}	width of flank wear land
v_c	cutting speed
V_c	cutting volume
α	tool orthogonal clearance
β	resulting angle of λ and τ
γ	rake angle
λ	feed angle
τ	tilt angle (milling)
ψ	tilt angle (residual stress measuring)
Θ	Bragg angle
σ_{max}	maximal principal residual stress

1. Introduction

In order to achieve the global climate goals, it is necessary to reduce CO₂ emissions and increase the efficiency of plants,

machines and transportation. Particularly for moving and rotating components, e.g., in turbines, lightweight materials are required to face this challenge [1]. Such materials are often exposed to high temperatures, and should provide a high strength at a low material density and high resistance against corrosion and wear. At the same time high safety standards have to be met. In recent years, innovative concepts of intermetallic alloys with Al and a transition metal have been developed; iron and titanium aluminides are becoming increasingly important [2]. The combination of high-strength material properties, low density and major advantage of undemanding availability of the two main alloying elements of FeAl alloys enable mass savings and show potential for applications in the areas of mobility and energy conversion. In particular, the flow stress anomaly or high yield strength at elevated temperatures of some FeAl alloys favors their suitability as substitutes for conventional high-temperature materials such as Ni alloys or creep resistant steels [2].

While an extensive database of systematic analyses already exists for conventional high-temperature materials in aircraft construction (e.g., IN718, Ti-6Al-4V) there is little information available for FeAl alloys considering the entire process chain or processing strategies [3, 4]. FeAl alloys with coherent continuous precipitates (e.g., FeAlTa) have already been investigated in recent studies for sand and investment casting showing promising results [5]. The possibility of added value by increasing productivity and component performance justifies investigations of casting properties in permanent mold casting – and subsequent machinability – compared to sand or investment casting. Permanent mold casting is characterized by higher cooling rates and thus, faster solidification processes of the material, causing a finer microstructure and potentially improved properties. However, a higher cracking risk due to the high-strength and low-ductility-behavior in combination with hard precipitates and the rather brittle behavior at room temperature involving a difficult machinability are challenging, e.g., causing increased process forces, tool wear and reduced surface quality. The surface integrity is mainly characterized by the topographical, mechanical and metallurgical influence on the surface layer and their interactions [6]. Surface defects (chipping, cracks, material buildup, etc.), high roughness or degraded properties due to metallurgical alterations of the surface layer can usually be attributed to premature tool wear or inadequate milling parameters. Thus, adequate tool and machining parameters have to be selected for the manufacturing of safety-relevant components. High tensile residual stresses at or below the surface may also be detrimental to the fatigue, premature failure or cracking behavior [7].

These challenges in finishing can be met with modern hybrid machining processes. In ball-end milling of hard, brittle materials, the superposition of the cutting process with ultrasonic oscillation in the direction of the rotating axis has already been successfully applied [8]. Ultrasonic-assisted milling (USAM) showed significantly reduced process forces and temperatures and, hence, significantly lower loading on the component surface and the tool cutting edge. In a research project involving Access e.V. and BAM, the machinability by means of USAM of FeAl components produced by means of permanent mold casting is being investigated.

2. Experimental

2.1. Material preparations

In 2014, Li et al. [9] highlighted the beneficial mechanical properties of FeAl alloys with additions of Ti, B and Mo, due to a DO_3 -ordered Fe_3Al matrix with complex Mo_2FeB_2 -type phase at grain boundaries at 650 °C, significantly increasing the creep-strength at a sufficient ductility. The alloy Fe26Al4Mo0.5Ti1B [at. %] shows good mechanical properties at moderate temperatures (500–550 °C) and excellent corrosion resistance in oxidic and sulphidic media. The addition of Mo and Ti leads to the stabilization of the ordered DO_3 phase and, thus, to an increase of the critical transition temperatures $T_c^{D03 \leftrightarrow B2}$ and $T_c^{B2 \leftrightarrow A2}$. It has incoherent precipitates, e.g., carbides or borides. Compared to investment casting providing geometries close to the final contour, gravity die casting requires a significantly larger oversize, which has to be removed by means of finish machining.

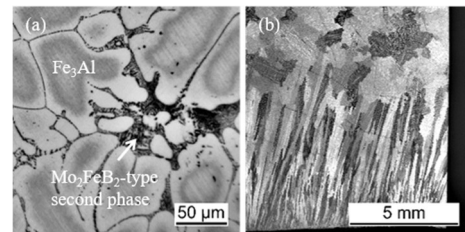


Fig. 1. Micrographs of (a) the microstructure of Fe_3Al -matrix with Mo_2FeB_2 -type second phase and (b) typical grain structure of gravity die casting of Fe26Al4Mo0.5Ti1B [at. %] in as-cast condition.

The design of the casting process for specimen production and determination of the casting properties were carried out by Access e.V. using the centrifugal casting process on a LINN Supercast casting plant. An induction coil heats the alloy Fe26Al4Mo0.5Ti1B [at. %] in a ceramic crucible under Ar atmosphere to an overheating of 60 °C above the melting temperature (approx. 1454 °C). Casting is carried out under vacuum with preheated (100 °C) copper molds.

2.2. Milling experiments

The milling experiments were performed on a five-axis machine (DMU 65, by DMG-MORI) shown in Figure 2, which is modified for the USAM process. Cooling lubricant Rhenus FY 121 L was used. The effective ultrasonic oscillation of the tool was analyzed at the tool tip via a laser vibrometer. During the milling experiments, a multi-component dynamometer (9139AA, by. Kistler) permitted in-situ cutting force analysis with an incremental time step length of 0.02 ms. For all force components (feed force F_f in the x -direction, feed normal force F_{fN} in the y -direction and passive force F_p in the z -direction) the integral from each individual cutting engagement of the tool was determined and the resulting force F_r was calculated using Eq. 1, in order to compare the effect of the individual input parameters:

$$Fr = \sqrt{F_f^2 + F_{fN}^2 + F_p^2} \quad (1)$$

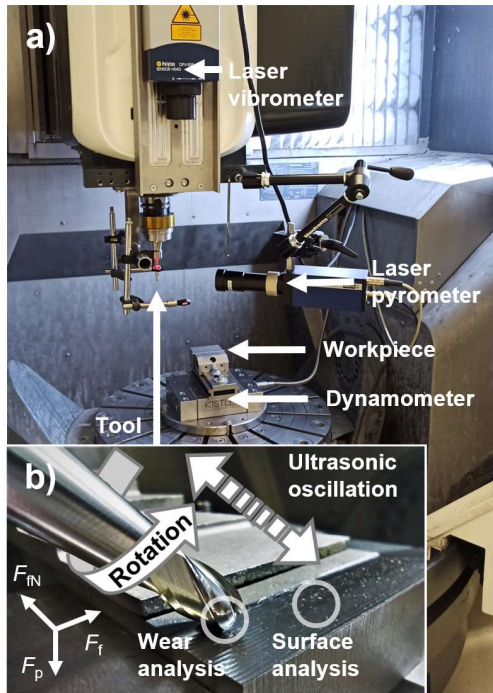


Fig. 2. Experimental setup for milling tests with a) equipment for the measurement of the triaxial force (dynamometer), the ultrasonic oscillation (laser vibrometer) and b) schematic illustration of the process kinematics.

2.3. Tool and milling parameters

The experimental procedure was performed with the standard parameter set with $v_c = 70$ m/min and $f_z = 0.055$ mm/tooth, cf. Table 1. To investigate the influence on the residual stresses of the surface, a parameter variation of the cutting speed v_c (30 and 110 m/min) and the tooth feed f_z (0.04 and 0.07 mm/tooth) were applied. In addition, conventional milling (0% USAM) was compared with ultrasonic-assisted milling (100% USAM). A volume of 2500 mm³ was removed during each tool test. The rotational speed n for the ball end milling cutter is calculated from v_c , the feed angle λ and tilt angle τ according to [3].

Table 1. Cutting parameters used during the machining experiments.

Feed angle: $\lambda = 45^\circ$	Depth of cut: $a_p = 0.3$ mm
Tilt angle: $\tau = 45^\circ$	Step over: $a_c = 0.3$ mm
Ultrasonic frequency: $f_{US} = 38.1$ kHz \pm 0.4 kHz	Ultrasonic amplitude: $A_{US} = 3$ μ m \pm 15%
Cutting speed: $v_c = 30, 70$ and 110 m/min	Feed per cutting edge: $f_z = 0.04, 0.055$ and 0.07 mm/tooth

The development of a suitable tool technology is based on a prototype tool developed by Fa. Wolf GmbH, which is a AlTiCrN PVD multilayer coated (thickness of approx. 2–3 μ m, hardness approx. 3300 HV0.5) solid carbide full radius milling cutter with a diameter of 6 mm with four cutting edges (tool no. 0 in Table 2). The parameters of the tool geometry in Table 2 relate to the ISO 3002. The variations of the rake angle γ refer to the first rake face at the cutter periphery at the 45° position on each of the four cutting edges of the full radius milling tool. The values of the tool orthogonal clearance α refer to the 300 μ m wide first clearance face. The second clearance angle is 35° for all the tools used. Initial tests with the prototype

tool no. 0 showed a steady increase of the resulting cutting force with continuous material removal. This consistent increase is due to the steadily growing tool wear and the associated blunting of the cutting edges. Mainly minor chipping occurs along the cutting edges. Hardly any scoring or other damage to the coating is observed along the breakout edges. Therefore, it is assumed that the AlTiCrN coating is suitable for this application and purposeful for the further steps of tool development. On the basis of tool no. 0, a test matrix of five prototype tools for the identification of adequate tool properties is set up for the experiments, cf. Table 2.

Table 2. Properties of investigated prototype tools.

Tool no.	Geometry			Substrate		
	γ [°]	α [°]	r_β [μ m]	K_{IC} Shetty [MPa*m ^{1/2}]	Hardness [HV30]	Flexural strength [MPa]
0	5	15	none	EMT210	10.0	4200
1	2	15	none	EMT210	10.0	4200
2	0	12	none	EMT210	10.0	4200
3	0	12	10	EMT210	10.0	4200
4	0	12	none	CTS24Z	11.3	4000
5	0	12	none	K41UF	11.0	4400

As part of the adjustment of the macro geometry, the rake angle γ and tool orthogonal clearance α are gradually reduced (tool no. 1 and 2), resulting in an increase in the wedge angle and thus stabilization of the cutting edge. With the intention to prevent initial wear in the form of chipping along the sharp tool edge, the microgeometry of tool no. 3 is adapted by applying a defined cutting edge rounding of $r_\beta = 10$ μ m. In the following tool variants (no. 4 and 5), alternative carbide substrates (CTS24Z and K41UF) are tested as tool substrates with higher critical stress intensity factors K_{IC} (Shetty) to reduce the sensitivity to cracking and chipping.

2.4. Surface Analysis

To investigate the surface topography, the milled surfaces were examined by scanning electron microscopy (SEM, Phenom XL, Thermo Fisher Scientific), light optical microscopy (LOM, Keyence VHX-7000) and Nanofocus μ surf expert confocal microscope with the 800XS 20x objective with a calculated lateral optical limiting resolution of 0.48 μ m. Optical measurements are performed on five 1 mm² stitched measuring fields according to DIN EN ISO 25178 with a low-pass filter $S = 2$ μ m and a high-pass filter $L = 1$ mm. For the quantitative evaluation and comparison of the individual parameter constellations, the arithmetical mean height of the surface S_a is used, which represents an area-related extension of the conventional one-dimensional arithmetic mean R_a of the line roughness.

The residual stresses of the surface layer generated by tool no. 0 and varying the parameters v_c, f_z and ultrasonic assistance (see Table 2) were analyzed by means of X-ray diffraction (XRD, cf. Table 3 for measurement and mechanical parameters).

Table 3. Parameters for XRD residual stress analyses of specimen surfaces.

Measuring mode:	$\sin^2\psi$	Collimator φ :	3 mm
Radiation:	Cr-K α	Tube power:	30 kV / 6.7 mA
Detector:	Linear solid-state	ψ -tilting:	0° to $\pm 45^\circ$
Diffraction line:	{211} α	ψ -step:	9
2 Θ -angle:	149°	Measuring time:	5 s
Young modulus E :	170 GPa [13]	Poisson's ratio ν	0.31 [13]

3. Results and discussion

3.1. Process forces

At the beginning of the machining experiments after a volume of material removal of 500 mm³, no significant effects of the tool on the resulting cutting force F_r are observable, cf. Figure 3. The reduction of the rake angle for tools no. 1 to 5 as a measure to stabilize the cutting edge led to a slight increase in the forces compared to the standard tool no. 0.

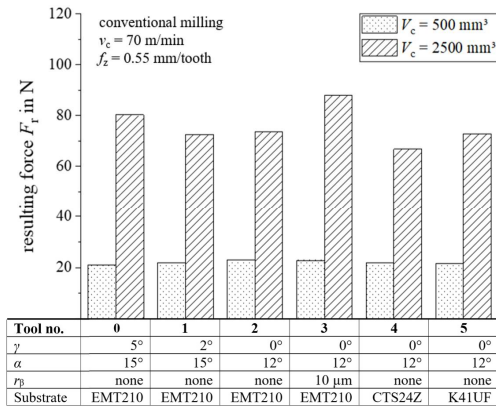


Fig. 3. Resulting force F_r of the individual prototype tools no. 0–5 at the beginning and at the end of the experiments.

With a volume of material removal of 2500 mm³, on the other hand, significant differences in the resulting cutting force can be observed. This is due to the differently pronounced wear of the respective tool numbers in the form of blunting and damage to the cutting edges. On the basis of the resulting force F_r for each individual tool, the suitability of the respective tool properties can already be evaluated according to the total metal removal rate. The geometry of tool no. 1 with a rake angle of 2° appears to be particularly suitable due to the low forces that occur. Tool no. 4 with the substrate CTS24Z and the same geometry as tool no. 2 shows the lowest values. The rounding of the cutting edge in tool no. 3 results in a significant increase in the resulting cutting force.

3.2. Tool wear

The evaluation of the maximum width of the flank wear land VB_{max} (LOM analysis) for all four cutting edges of all tools in Figure 4 shows several significant differences between the individual prototype tools. The lowest wear of the prototype tools no. 1–5 exhibits tool no. 1, as the other tools each show higher wear values compared to the initial tool. Tool no. 4 also shows a positive trend despite the rather unsuitable geometry

(cf. tool no. 2), which can be related to the alternative substrate CTS24Z. With the measurement of the wear area on the flank faces of each of the four tool cutting edges, the positive wear behavior of tool no. 4 becomes more obvious. The reduced wear effect of tool no. 1 and 4 correlates with the reduced resulting forces (after a volume of material removal of 2500 mm³) of both tools during the milling experiments.

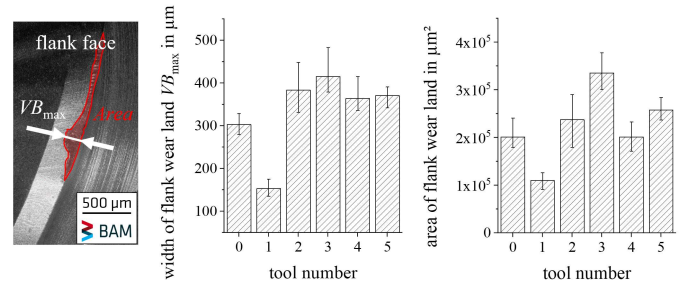


Fig. 4. Tool wear measured by mean value of area and width of flank wear land VB_{max} of the four cutting edges of each tool after $V_c = 2500$ mm³.

3.3. Surface integrity

3.3.1 Topography

The effect of the USAM on the surface topography shown in SEM images in Figure 5 was already observed using tool no. 0. The surfaces machined by ultrasonic-assisted milling as often observed in other studies [8, 10, 12] appear more homogeneous and show fewer imperfections.

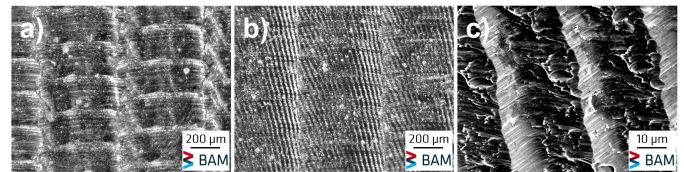


Fig. 5. SEM images of surfaces after experiments for a) CM and b) USAM; detail of the pattern due to ultrasonic oscillation of the tool (c)

The stabilization of the cutting wedge by reducing the rake angle from 5° to 2° in tool no. 1 results in the lowest S_a values of all tool variants in Figure 6, which can be attributed to its low wear. With the cutting edge rounding in tool no. 3, low S_a values are also achieved. However, this is due to the smearing effect of the cutting edge rounding $r_\beta = 10$ μ m as well as blunting due to wear (see Figure 4). The advanced wear of tool no. 3 produces visible surface defects due to the irregular material removal of the damaged cutting edges. However, the S_a value is often not capable of representing these defects of a surface, which is why an additional qualitative evaluation and further analysis methods are required. Figure 6 shows the surfaces produced by each tool and an evaluation of the severity and count of surface defects. These defects, typical of tool wear in the form of material buildup and breakout, are shown in detail in Figure 7.

With a further reduction of the rake angle from 2° to 0° as well as the tool clearance from 15° to 12° in tool no. 2, many of these wear-related defects also occurred. Here, the increased friction due to the enlarged contact area between the workpiece and the flank face is probably the reason for the negative effect in terms of tool wear and resulting surface integrity.

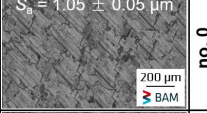

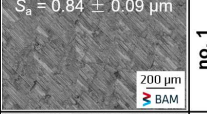
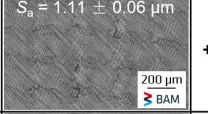
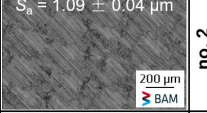
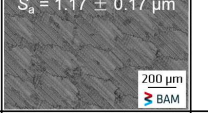


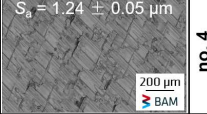



Defects		CM	Tool	USAM	Defects	
count	severity				count	severity
+	+	$S_a = 1.05 \pm 0.05 \mu\text{m}$  200 μm BAM	no. 0	$S_a = 1.17 \pm 0.04 \mu\text{m}$  200 μm BAM	+	++
++	++	$S_a = 0.84 \pm 0.09 \mu\text{m}$  200 μm BAM	no. 1	$S_a = 1.11 \pm 0.06 \mu\text{m}$  200 μm BAM	+++	+++
+	+	$S_a = 1.09 \pm 0.04 \mu\text{m}$  200 μm BAM	no. 2	$S_a = 1.17 \pm 0.17 \mu\text{m}$  200 μm BAM	++	+
+	+	$S_a = 0.94 \pm 0.05 \mu\text{m}$ Material buildup  200 μm BAM	no. 3	$S_a = 0.92 \pm 0.06 \mu\text{m}$ Material breakout  200 μm BAM	+	+
+	++	$S_a = 1.24 \pm 0.05 \mu\text{m}$  200 μm BAM	no. 4	$S_a = 1.17 \pm 0.08 \mu\text{m}$  200 μm BAM	++	+++
+	+	$S_a = 1.31 \pm 0.05 \mu\text{m}$  200 μm BAM	no. 5	$S_a = 1.43 \pm 0.09 \mu\text{m}$  200 μm BAM	++	+

Fig. 6. Comparison of the surfaces produced by tool no. 0 to 5 respectively by conventional (CM) and ultrasonic-assisted milling (USAM) after a cutting volume of 2500 mm³ ($v_c = 70$ m/min and $f_z = 0.055$ mm/tooth); assessment of defects: “+” high count/severity to “+++” low count/severity.

The values of the reduced peak height S_{pk} calculated from the Abbott-Firestone curve according to the ISO 25178-2 standard clearly show these undesirable effects on the surface due to tool no. 2 and 3 in Figure 8. Despite the same unsuitable geometrical properties of tool no. 2, a significant reduction of S_{pk} could be achieved with the alternative substrate CTS24Z in tool no. 4, which provides a higher K_{IC} . Similar to the S_a values, the increased S_{pk} value with USAM is caused by the pattern due to the ultrasonic oscillation shown in Figure 5. With USAM, the substrate CTS24Z of tool no. 4 exhibits comparatively yet slightly increased S_{pk} values. The alternative substrate K41UF in tool no. 5 did not show positive results in terms of process forces, tool wear and thus surface integrity and will therefore not be purposeful in further investigations.

Even though the S_{pk} and S_a values shown here are increased with USAM, a considerable positive effect in terms of low defect density is observable, cf. Figure 6. Together with significantly reduced tool wear during preliminary tests with USAM, resulting surface residual stresses (cf. section 3.3.2) and in context with a number of investigations of other authors [8, 10, 12], these positive effects on the surface integrity, and of the tool properties, motivate the development of tools specialized for USAM for those hard-to-cut intermetallic alloys. Therefore, the combination of the generally positive geometric properties of tool no. 1 with the substrate CTS24Z (tool no. 4) is identified to be appropriate to produce a prototype tool for further investigations regarding the optimization of the milling process and surface integrity using USAM.

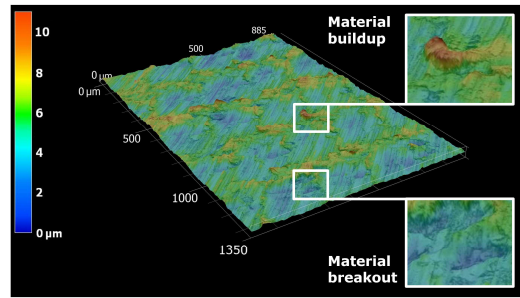


Fig. 7. Typical tool wear-related material buildup and breakout evident in the topography of the surface produced by tool no. 3 with CM at $v_c = 70$ m/min and $f_z = 0.055$ mm/z after $V_c = 2500$ mm³.

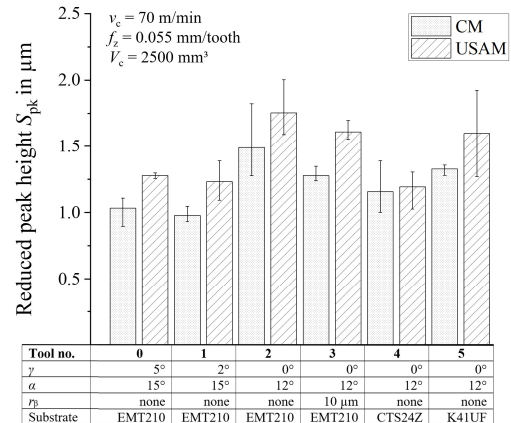


Fig. 8. Reduced peak height S_{pk} produced by each tool after a volume of material removed of $V_c = 2500$ mm³ with CM and USAM.

3.3.2 Surface residual stresses

Residual stresses are the consequence of inhomogeneous plastic deformation. In milling processes, these result from mechanical forces between the tool cutting edge and the workpiece and from local heating of the surface above the temperature-dependent local material yield strength. Both mechanisms produce typical residual stress depth profiles with balanced tensile and compressive stresses [10]. Tensile residual stresses at the surface layer are undesirable for highly stressed safety-relevant surfaces, as they may be detrimental regarding crack initiation or formation causing premature failure [7]. Other studies exhibited a beneficial influences of USAM on the surface residual stresses, e.g., for multiple principal element alloys or NiCr alloys [8, 10, 12]. Figure 9 shows the max. principal residual stresses σ_{max} determined by three measurements in different angles with respect to the x -direction (0°, 45°, 90°) of the milled surfaces for USAM and CM, and the initial condition. The initial specimen surface exhibits compressive residual stresses due to sandblasting as material preparation after casting. It is shown that low cutting speeds and tooth feeds lead to a lower input of tensile residual stresses, as reported by other authors [10]. With higher tooth feed as well as cutting speed, a maximum of residual stresses is achieved with the central parameters. With further increase of cutting speed and tooth feed, slightly lower tensile residual stresses are present, which can be explained by a lower heat exposure of the workpiece surface, since more process heat is dissipated via the chip removal. Significant beneficial effects of USAM on the reduction of tensile residual stresses on the surface layer are

obvious. As described by other authors [8], USAM reduces the friction in the cutting process between tool and workpiece. The superimposed ultrasonic motion of the cutting edge leads to a reduction in the contact time of the cutting engagement and heat transfer in the process zone, which ultimately results in lower thermo-mechanical stress due to heat transfer and plasticization. In addition, the ultrasonic oscillation component causes a sort of impact effect similar to shot peening, which results in densification of the surface layer and in an increase in residual compressive stresses. This could be also confirmed for the machining of FeAl and should be the focus of future investigations.

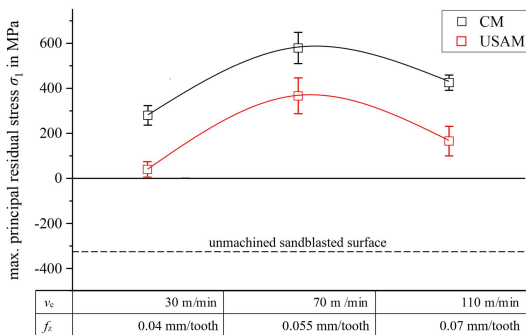


Fig. 9. Comparison of maximum principal residual stresses σ_{\max} at the surface layer for minimal, central, maximum milling parameters for CM and USAM (using tool no. 0.)

4. Conclusion and Outlook

Due to its advantageous mechanical and lightweight properties and the availability of its alloying components, iron aluminide has a market potential to substitute conventional high temperature materials. However, this requires the development of a holistic, economical production route from casting to finishing machining, which must meet highest safety requirements for component integrity and, therefore, surface integrity. This may be achieved using USAM process for ball-end milling, which can significantly reduce the load on the surface as well as on the tool. First experimental results of an ongoing investigation are shown and summarized as follows:

- (1) Suitable tool properties were identified and will be the basis of further investigations. To counteract the impact loads on the cutting edge, the cutting wedge must be stabilized by reducing the rake angle and using tool substrates that are insensitive to cracking. The next step of tool prototype development will be a combination of the geometry from tool no. 1 and substrate from tool no. 4.
- (2) With a further reduction of the tool orthogonal clearance, tool wear increased, and the surfaces produced were of lower quality. A rounding of the cutting edge exhibits lower S_a values, but a significantly higher amount and severity of defects due to considerably increased tool wear.
- (3) Positive effects of USAM can be confirmed in this study regarding the reduction of surface residual stresses, and the topography appearing more homogeneous and with a lower defect density and severity. However, this rather qualitative observation was not reflected by conventional characteristic values (S_a , S_{pk}) and should be confirmed by appropriate quantitative methods in future investigations.

- (4) The variation of the parameters used in the experiments should enable an optimum design of the milling process to find economic and safe machining parameters for the aimed FeAl alloy system based on an extended and reproducible experimental matrix and data base.

Acknowledgements

The research project is being carried out as part of the "Central Innovation Program for SMEs" (ZIM, ZF4044235), funded by the Federal Ministry for economic Affairs and Climate Action (BMWK) on the basis of a decision by the German Bundestag.



We would like to thank for this support. Furthermore, the authors want to thank Daniel Stock, Marina Marten, Christina Neumann and Karsten Zieger for their technical support.

References

- [1] International Air Transport Association (IATA), Aircraft Technology Roadmap to 2050. <https://www.iata.org/contentassets/8d19e716636a47c184e7221c77563c93/Technology-roadmap-2050.pdf> (accessed on 18.03.2022)
- [2] M. Zamanzade, A. Barnoush, C. Motz. A Review on the Properties of Iron Aluminide Intermetallics. *Crystals* 6(1); 2016.
- [3] B. Denkena, D. Nesper, V. Böß, J. Köhler. Residual stresses formation after re-contouring of welded Ti-6Al-4V parts by means of 5-axis ball nose end milling. *CIRP Journal of Manufacturing Science and Technology* 7(4); 2014. p. 347-360.
- [4] A. Thakur, S. Gangopadhyay. State-of-the-art in surface integrity in machining of nickel-based super alloys. *International Journal of Machine Tools and Manufacture* 100; 2016. p. 25-54.
- [5] D.D. Risanti, G. Sauthoff. Microstructures and mechanical properties of Fe–Al–Ta alloys with strengthening Laves phase. *Intermetallics* 19(11); 2011. p. 1727-1736.
- [6] D. Ulutan, T. Ozel. Machining induced surface integrity in titanium and nickel alloys: A review. *International Journal of Machine Tools and Manufacture* 51(3); 2011. p. 250-280.
- [7] R. M'Saoubi, J.C. Outeiro, H. Chandrasekaran, O.W. Dillon Jr, I.S. Jawahir. A review of surface integrity in machining and its impact on functional performance and life of machined products. *International Journal of Sustainable Manufacturing*; 2008. p. 203-236.
- [8] D. Schroeffer, K. Treutler, A. Boerner, R. Gustus, T. Kannengiesser, V. Wesling, W. Maus-Friedrichs. Surface finishing of hard-to-machine cladding alloys for highly stressed components. *International Journal of Advanced Manufacturing Technology*; 2021. p. 1427–1442.
- [9] X. Li, P. Prokopčáková, M. Palm. Microstructure and mechanical properties of Fe–Al–Ti–B alloys with additions of Mo and W. *Materials Science & Engineering A* 611; 2014. p. 234-241.
- [10] T. Richter, D. Schroeffer, M. Rhode, A. Boerner, R.S. Neumann, M. Schneider, G. Laplanche. Influence of machining on the surface integrity of high- and medium-entropy alloys. *Materials Chemistry and Physics* 275; 2022.
- [11] M. Wagner, H. Michels, C. Hamm, M. Appelt, T. Roeser, M. Weigold. Influence of tool variables on wear when milling iron aluminide alloy Fe25Al1.5Ta [at.-%]. *Procedia Manufacturing* 40; 2019. p. 1-7.
- [12] A. Suárez, F. Veiga, L.N. Lacalle, R. Polvorosa, S. Lutze, A. Wretland. Effects of Ultrasonics-Assisted Face Milling on Surface Integrity and Fatigue Life of Ni-Alloy 718. *Journal of Materials Engineering and Performance*; 2016. p. 5076–5086.
- [13] Y. Zheng, F. Wang, T. Ai, C. Li. Structural, elastic and electronic properties of B2-type modified by ternary additions FeAl-based intermetallics: First-principles study. *Journal of Alloys and Compounds* 710; 2017. p. 581-588.